High Spatial and Temporal Resolution Cardiac Cine MRI from Retrospective Reconstruction of Data Acquired in Real Time Using Motion Correction and Resorting

Peter Kellman,[1] Christophe Chefd'hotel,[2] Christine H. Lorenz,[3] Christine Mancini,[1] Andrew E. Arai,[1] and Elliot R. McVeigh[4]

Cine MRI is used for assessing cardiac function and flow and is typically based on a breath-held, segmented data acquisition. Breath holding is particularly difficult for patients with congestive heart failure or in pediatric cases. Real-time imaging may be used without breath holding or ECG triggering. However, despite the use of rapid imaging sequences and accelerated parallel imaging, real-time imaging typically has compromised spatial and temporal resolution compared with gated, segmented breath-held studies. A new method is proposed that produces a cardiac cine across the full cycle, with both high spatial and temporal resolution from a retrospective reconstruction of data acquired over multiple heartbeats during free breathing. The proposed method was compared with conventional cine images in 10 subjects. The resultant image quality for the proposed method (4.2 ± 0.4) without breath holding or gating was comparable to the conventional cine (4.4 ± 0.5) on a five-point scale (*P* = n.s.). Motion-corrected averaging of real-time acquired cardiac images provides a means of attaining high-quality cine images with many of the benefits of real-time imaging, such as free-breathing acquisition and tolerance to arrhythmias. Magn Reson Med 62:1557–1564, 2009. © 2009 Wiley-Liss, Inc.

Key words: MRI; heart; real-time; parallel MRI; SENSE; navigator; motion correction; nonrigid; myocardial function

Cine MRI is used for assessing cardiac function and flow and is typically based on a breath-held, segmented data acquisition (1-5). Breath holding is particularly difficult for patients with congestive heart failure or in pediatric cases. Real-time imaging may be used without breath holding or ECG triggering (6-9). However, despite the use of rapid imaging sequences and accelerated parallel imaging (10-13), real-time imaging typically has compromised spatial and temporal resolution compared with gated, segmented breath-held studies. A new method is proposed that produces a cardiac cine across the full cycle, with both high spatial and temporal resolution from a retrospective reconstruction of data acquired over multiple heartbeats during free breathing. Images were acquired in real time in a nontriggered manner, and cardiac phase binning was performed retrospectively, based on the recorded R-wave triggers.

Free-breathing cardiac imaging with respiratory gating may be implemented using navigator echoes (14,15), which track the position of the diaphragm. Data are accepted or rejected based on an acceptance window. Prospective slice-following techniques (16) improve the image quality by adjusting for heart motion within the acceptance window, thereby allowing a somewhat increased window with higher acquisition efficiency. However, the motion of the heart does not strictly track the diaphragm during free breathing (17), which limits the dependence on simple models and linear motion correction factors. Furthermore, use of conventional navigator echoes is problematic for continuous cine imaging due to the overhead time required to generate the navigator signal and due to interruption of the steady state. Respiratory self-navigator approaches have been demonstrated for cardiac cine imaging using radial acquisition (18,19), as well as three-dimensional Cartesian (20,21), which relies on profiles derived by repeated sampling through the center of *k*-space. Nevertheless, dependence on a simple motion model still limits the image quality. A method for prospective self-gating that simultaneously compensates for cardiac and respiratory motion has recently been reported (22).

In previous work (23), real-time acquired images were temporally interpolated gaining an effective SNR gain but not improving the true temporal resolution. In this work, the complex data are not interpolated but rather rebinned to achieve the improved temporal resolution. The proposed method is compared with conventional segmented, breath-held cine imaging in 10 subjects.

MATERIALS AND METHODS

Proposed Strategy

Retrospective reconstruction of cine MRI was performed using data acquired in real time over multiple heartbeats during free breathing without ECG triggering. The strategy (Fig. 1) was based on acquiring images at the desired high spatial resolution with reduced temporal resolution, and retrospectively reconstructing high-temporal-resolution images following respiratory motion correction and rebinning of data over multiple heartbeats (details follow). Due to the asynchronous sampling of the image data with respect to the heart beating, the density of phase encodes at a given cardiac phase increases as a function of number of

[1]Laboratory of Cardiac Energetics, National Heart, Lung and Blood Institute, National Institutes of Health, DHHS, Bethesda, Maryland, USA

[2]Siemens Corporate Research, Princeton, New Jersey, USA

[3]Siemens Corporate Research, Baltimore, Maryland, USA

[4]Department of Biomedical Engineering, Johns Hopkins University, Baltimore, Maryland, USA

*Correspondence to: Peter Kellman, PhD, Laboratory of Cardiac Energetics, National Institutes of Health, National Heart, Lung, and Blood Institute, 10 Center Drive, MSC-1061, Building 10, Room B1D416, Bethesda, MD 20892-1061. E-mail: kellman@nih.gov

Received 3 April 2009; revised 15 June 2009; accepted 25 June 2009.

DOI 10.1002/mrm.22153

Published online 24 September 2009 in Wiley InterScience (www.interscience.wiley.com).

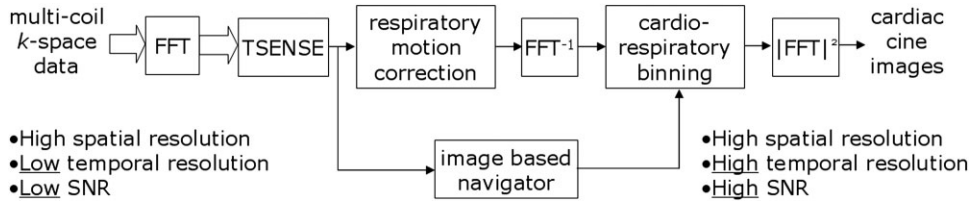

FIG. 1. Strategy for high-resolution retrospective reconstruction of cine MR images acquired in real time for multiple heartbeats without triggering. Images are acquired at the desired high spatial resolution with reduced temporal resolution, and high-temporal-resolution images are retrospectively reconstructed following respiratory motion correction and rebinning of data over multiple heartbeats.

heartbeats acquired, provided that data from multiple heartbeats can be appropriately combined and satisfy asynchrony requirements (Fig. 2). In this way, given a sufficient amount of data, a fully sampled dataset may be realized with higher temporal resolution.

Combining data acquired from different heartbeats requires that all the heartbeats be sufficiently similar or that retrospective arrhythmia rejection be used. It further assumes that the data are at a fixed respiratory phase or that respiratory motion is corrected. A fully automatic, retrospective, image-based respiratory navigator is used to limit the acceptance of data to a relatively small range of respiratory motion, and fine correction of any residual in-plane motion is performed using nonrigid image warping. For example, images were acquired for 60 sec at the desired spatial resolution (256 × 144 matrix) with a low temporal resolution of approximately 110 ms. The *k*-space samples were rebinned retrospectively after respiratory motion correction to enable a true temporal resolution of 33 ms without view sharing. It is assumed that there is very little respiratory motion during the 110-ms image frame (see Discussion).

The steps for this approach are:

(1) acquire time-stamped raw data using a real-time sequence and record timing for ECG R-wave triggers.

(2) reconstruct raw real-time images using parallel imaging

(3) produce an image-based navigator signal (23) and respiratory gating signal

(4) calculate the motion field to be used for subsequent motion correction

(a) cardiac gate the magnitude of the raw real-time images (23) using recorded ECG trigger times
(b) select reference heartbeat at end-expiration based on the navigator signal
(c) perform nonrigid motion registration for each cardiac phase and heartbeat using the previously selected reference heartbeat and output the motion field for each heartbeat and cardiac phase

(5) apply warping using the motion field to correct in-plane respiratory motion for each raw real-time acquired complex image at the corresponding cardiac phase and heartbeat

(6) transform the motion-corrected (warped) complex images back to *k*-space using FFT

(7) bin each readout according to output cardiac phase bins

(8) use respiratory gating and optional arrhythmia rejection to exclude some lines of *k*-space

(9) combine data in the same output cardiac phase bin for each PE line by averaging

(10) transform the *k*-space data to create the final higher temporal resolution cardiac cine images

Real-Time Imaging

Real-time imaging was performed on 1.5T Siemens Avanto and Espree scanners (Siemens Medical Solutions, Erlan-

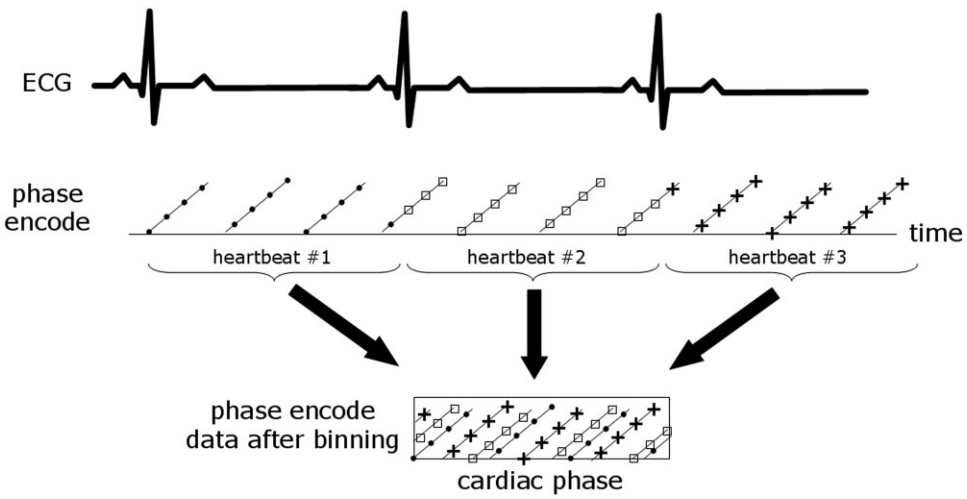

FIG. 2. Illustration of phase encode data vs cardiac phase after rebinning the real-time acquired data from multiple heartbeats. The density of samples increases with more heartbeats due to asynchrony between imaging and the heart cycle.

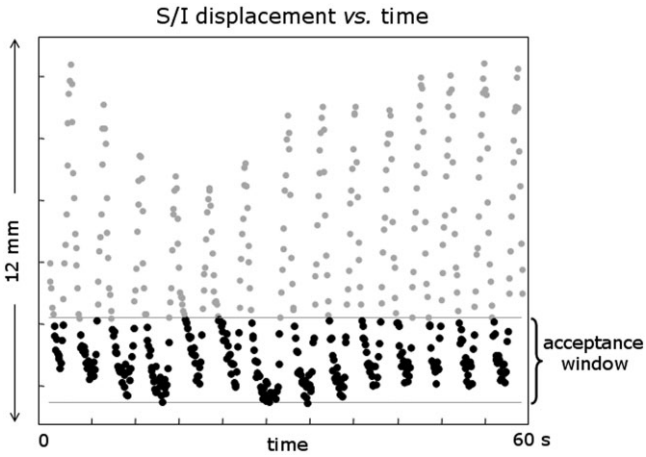

FIG. 3. Example image-based navigator signal derived from the motion field used to warp the real-time acquired images to the initial reference frame. The respiratory gating acceptance window is indicated. The horizontal time axis spans 60 sec and the vertical axis is tissue displacement spanning 12 mm.

gen, Germany), using a balanced SSFP (true-FISP) sequence. Parallel imaging was used to provide rate four acceleration using sensitivity encoding (SENSE) (10) incorporating temporal filtering for auto-calibration (TSENSE) (12). The initial temporal resolution was approximately 110 ms for 256 × 144 matrix, BW = 977 Hz/pixel (pulse repetition time = 3.1 ms). The excitation flip angle was 50°. Images were acquired continuously without ECG gating for 60 sec during free breathing. Retrospective image reconstruction from raw data with embedded ECG timing data was performed off-line using MATLAB® (Mathworks, Natick, MA). Conventional breath-held segmented balanced SSFP cine imaging with the following parameters was used for comparison: matrix = 256 × 156, views per segment = 10, pulse repetition time = 3 ms, BW = 930 Hz/pixel, temporal resolution = 30 ms, with 30 phases calculated retrospectively, rate 2 parallel imaging using the GRAPPA method (11), and 11-heartbeat breath-hold duration. The image field of view was typically 360 × 270 mm^2 (75% rectangular field of view), which corresponded to a typical in-plane spatial resolution of 1.4 × 1.9 mm^2 for the 256 × 144 matrix. Slice thickness was 6 mm.

Image Registration

Image registration was used for calculating both the image-based navigator signal and for estimating the motion field used for respiratory motion correction. Nonrigid registration was performed pairwise between a target and reference image. Nonrigid registration was used since it could be fully automated over the full field of view without user interaction to specify bounding regions, and in previous application to motion-corrected late enhancement imaging, it outperformed rigid-body registration in the heart region (24). For each pair, the algorithm (25,26) estimates a deformation that maximizes the local cross-correlation between the reference and the uncorrected (target) image. The process is implemented in a multiscale approach from coarse to fine resolution (in four steps of two) which increases the speed and provides improved convergence. Once the nonrigid motion (deformation) field is estimated, the images are warped using a subpixel spline-based interpolator.

Navigator Signal

The image-based navigator signal was used to determine which data were to be accepted in the final image reconstruction. The image-based navigator signal was also used to determine which heartbeat was presumed to be at end-expiration to be used as a reference for image registration to estimate the motion field for respiratory motion correction. The navigator signal processing has previously been described (23). Respiratory gating had an acceptance window of 25% of the full-scale image-based navigator signal (Fig. 3). Following motion correction and transform back to *k*-space, resultant lines of *k*-space that were acquired at times falling outside the navigator acceptance window were excluded from the final reconstruction in the rebinning step.

Motion Correction

The lower-temporal-resolution, real-time, acquired-magnitude images were also used to calculate the motion field for subpixel in-plane respiratory motion correction. The nonrigid motion field for each real-time image frame is estimated by image registration of the real-time magnitude images with reference images from a heartbeat at end expiration. The target and reference images are from the same cardiac phase but at different heartbeats, and this process is repeated for each cardiac phase. Thus, prior to registration, the magnitude real-time images are first cardiac gated (23) such that the images could be selected by cardiac phase and heartbeat. The resultant motion field closest in time to the complex real-time image is then used to warp the complex raw real-time image (Fig. 4) using a spline interpolator. It is required to operate on the complex image since the warped images are transformed back to *k*-space for temporal rebinning and respiratory gating.

Data Rebinning

Motion-corrected complex images were transformed back to *k*-space by means of FFT, and individual readouts were rebinned according to cardiac phase subject to navigator

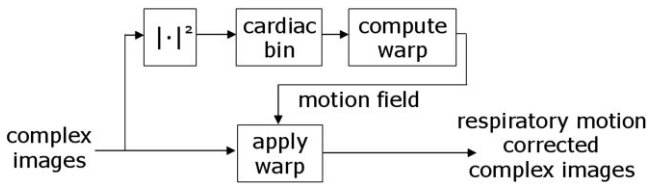

FIG. 4. Simplified processing diagram for respiratory motion correction of complex real-time acquired images. A nonrigid motion field for each real-time image frame is estimated by image registration of the real-time images with a fixed reference image (from a heartbeat at end expiration) for each cardiac phase. The motion field is then used to warp the complex images at the corresponding time.

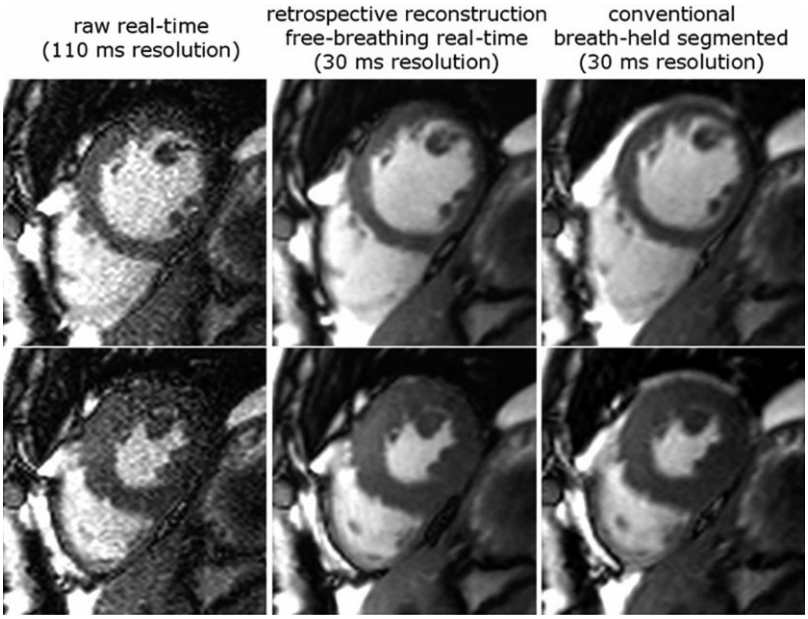

FIG. 5. Comparison of raw real-time acquired images (left), retrospective reconstructed images (center), and conventional (right) cine images.

signal-based respiratory gating. Retrospective arrhythmia rejection could be applied at this stage. Simple cardiac rebinning was performed that consisted of averaging all samples that fell within the specified output phase bin, where typically 30 output phases were calculated across the cardiac cycle (i.e., 33 ms for 60 bpm). Statistics were saved on the total number of samples and the total accepted samples per PE line and cardiac phase, as a function of how many heartbeats were acquired.

Although the data were acquired in real time without ECG triggering, the time of each readout (echo) was recorded with the raw data, as well as the time from the previous ECG R-wave trigger, with a precision of 2.5 ms. The ECG timing data were used for determining a cardiac phase using either linear or piecewise linear mapping (23,27). The time stamps were replaced by a linear fit, which virtually eliminates the 2.5-ms quantization error.

Experimental Measurements

Images were acquired and processed for $N = 10$ subjects, including patients ($N = 6$) with suspected coronary artery disease or known chronic myocardial infarction and healthy volunteers ($N = 4$) under clinical research protocols approved by the institutional review boards of the National Heart, Lung, and Blood Institute and Suburban Hospital, with written informed consent, and analysis approved by the NIH Office of Human Subject Research.

Retrospectively reconstructed images acquired in real time during free breathing were compared with conventional, breath-held, gated, segmented, cine imaging for a single slice (midventricular short axis slice for 10 subjects). Additionally, long-axis views were acquired in several subjects. Image quality for all subjects was assessed by two experts using a five-point scale (with increment = $\frac{1}{2}$) as described below, and statistical significance was assessed using a paired t test. Conventional breath-held, ECG-gated, segmented images and retrospectively reconstructed real-time acquired images for the corresponding slice were scored separately, presented in a blinded, randomized manner. The rating was based on (a) SNR and image artifacts, (b) readability of global function, (c) readability of regional function, and (d) ability to discern fine details such as chordal structures, valve leaflets, and LV trabeculation. A score of 5 (excellent) was assigned when all four aspects were rated as excellent, i.e., without artifacts, high contrast between blood and myocardium, and sharp borders and distinct appearance of fine structural details. A score of 4 (good) was assigned when all aspects were rated as good, with some fine structures visible, but not necessarily all, and possibly mild artifacts. A score of 3 (fair) meant that the images were sufficient to read regional wall motion but that one or more aspect of image quality were suboptimal. A score of 2 (poor) meant that one or more aspects were seriously impaired, leading to inability to read regional function. Images rated with a score of 1 were considered nondiagnostic when regional and global function could not be determined.

Endocardial contours at end-diastole and end-systole were manually traced for the short axis slices ($N = 10$ subjects) and the estimate of ejection fraction based on the single slice was compared for the two methods, using a paired t test. To further characterize the performance of the proposed method, statistics were computed on the average number of samples in each output cardiac phase bin as a function of PE line and number of heartbeats used.

RESULTS

Images (Fig. 5) are shown for end-diastolic and end-systolic phases comparing raw real-time (left), proposed retrospective reconstruction of free-breathing real-time acquired images (center) and conventional breath-held, segmented acquisition (right). The temporal resolution of the proposed retrospective reconstruction and conventional methods is the same, 30 ms in this example. The intensity profiles vs time (Fig. 6) (pseudo m-mode) for a profile

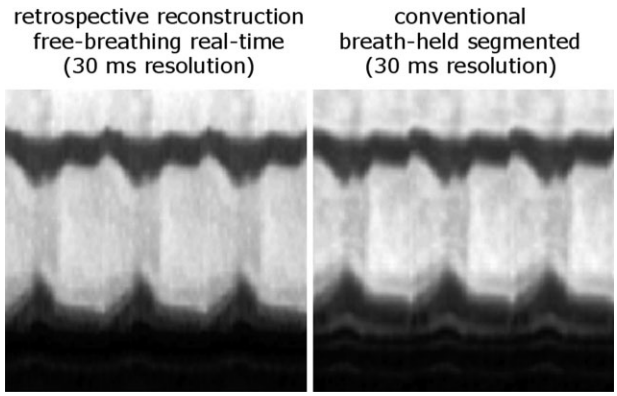

FIG. 6. Intensity profiles vs time (pseudo m-mode) for profile thru LV septum and free-wall comparing proposed (left) and conventional (right) cine imaging methods for case shown in Fig. 5.

through the LV septum and free-wall comparing proposed (left) and conventional (right) cine imaging methods are shown for the case of Fig. 5, demonstrating similarity of temporal characteristics. Fig. 7 shows a long-axis three-chamber view, with depiction of the mitral valve comparing several frames of raw real-time acquired images (top), retrospective reconstructed (bottom left), and conventional (bottom right) cine images. Note that the slice prescription for the conventional cine has a slight in-plane rotation as compared to the real-time data.

The proposed free-breathing method was compared with conventional breath-held cine images in 10 subjects. The resultant image quality for the proposed method (4.2 ± 0.4) without breath-holding or gating was comparable to the conventional cine (4.4 ± 0.5) on a five-point scale (P = n.s.). The estimated ejection fraction based on a single short-axis slice had average value $45.9 \pm 7.1\%$ for the conventional cine and $46.1 \pm 6.5\%$ for the proposed retrospective reconstruction method. There was no statistically significant difference as analyzed by paired t test (P = n.s.).

The k-space data fills in over time in an almost randomly appearing fashion, depending on the degree of asynchrony between the cardiac cycle and the temporal resolution of the raw real-time images. An example for one patient (Fig. 8) shows the k-space filling for multiple heartbeats (zoomed to show 1st 32 of 144 PE lines and 1st five of 30 output cardiac phases) acquired over 60 sec with initial temporal resolution of 110 ms and final resolution of 35 ms (at 57 bpm). The samples accepted by the respiratory gating signal are shown as black dots; the gray squares in the zoomed matrix represent all acquired samples. To characterize the filling of k-space vs acquisition duration, the maximum increment (or gap) in time for a fixed PE line (defined in Fig. 8) is plotted vs the number of heartbeats acquired (Fig. 9) for $N = 10$ subjects. Cardiac phase is defined here as number between 0 and 1 representing the time as a fraction of the R-R interval. Thus, for example, with 30 calculated output phases each cardiac phase bin would represent an increment of 1/30 in cardiac phase units. The dark lines correspond to the data accepted by the respiratory gating signal and the lighter gray lines represent all the data. The dashed horizontal line corresponds to 30 calculated output phases. The desired temporal resolution for all cardiac phases and PE lines was achieved with multiple copies of each phase encode in each cardiac phase bin for most subjects. In a single subject, the maximum cardiac phase increment for navigator gated data after 60-sec acquisition was $1/28.6 = 0.035$, which was slightly greater than the desired target of 1/30 heartbeats; nevertheless, the image quality in this case was still excellent. The maximum increment in cardiac phase between k-space samples was 0.02 ± 0.008 cardiac cycles (mean $\pm$ standard deviation, $N = 10$) for 60-sec acquisition. Multiple samples are averaged, yielding an improvement in SNR. The effective number of samples averaged over 60 sec of data collection was 7.9 ± 2.4 ($N = 10$) samples per output phase bin after respiratory gating corresponding to an average SNR improvement of $\sqrt{7.9} \approx 2.8$ above the SNR of the raw real-time acquired images. The SNR of the real-time acquired images using

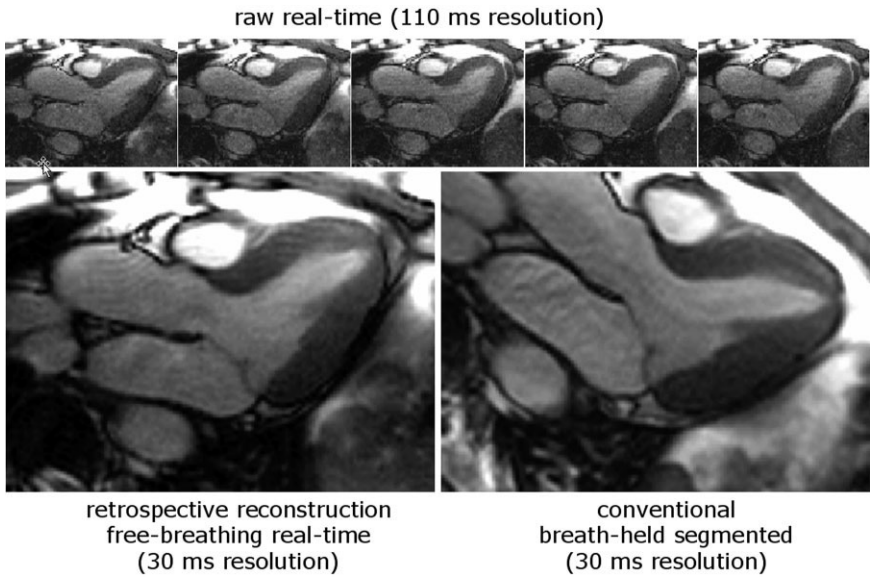

FIG. 7. Comparison of several frames of raw real-time acquired images (top), retrospective reconstructed (bottom left), and conventional (bottom right) cine images showing mitral valve in three-chamber long-axis view.

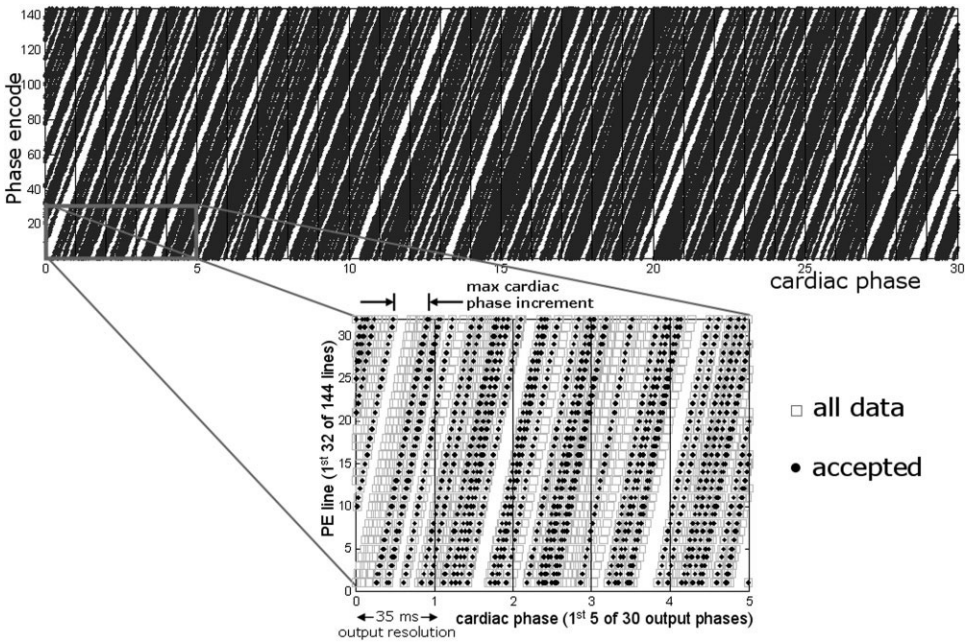

FIG. 8. Illustration of *k*-space filling showing *k*-space samples with multiple heartbeats (zoomed to show 1st 32 of 144 PE lines, and 1st five of 30 output cardiac phases) acquired over 60 sec, with initial temporal resolution of 110 ms and final resolution of 33 ms (at 57 bpm). The black dots represent samples that are accepted by the respiratory gating signal, and the gray squares (in the zoomed matrix) represent all the acquired data.

rate $R = 4$ parallel imaging acceleration with SENSE g-factor (10) approximately $g \approx 1.8$ (28) (using 32 coils), is approximately 2.5 worse than the conventional segmented cine using $R = 2$ ($g \approx 1$). Thus, the SNR of the retrospectively reconstructed images would be expected to be comparable to the conventional images in this example.

DISCUSSION

Real-time imaging is sufficiently fast to track respiratory motion, and images acquired during free-breathing may be motion corrected. An underlying assumption is that the respiratory motion is relatively small over the image duration of the initial lower temporal resolution real-time acquired image (approximately 100 ms), such that the lower temporal resolution motion field estimate will be sufficiently accurate to correct in-plane motion. The in-plane motion was found to be as high as 10 pixels over the full range of cardiorespiratory phase; however, the motion was significantly reduced to on the order of one to two pixels over the range of respiratory phase accepted based on the image-based respiratory navigator. Importantly, the rate of change for the navigator-accepted data was found to be subpixel, with <0.25 pixel rms over $\pm$ 50 ms. Thus, 100-ms resolution was deemed acceptable for the real-time acquisition.

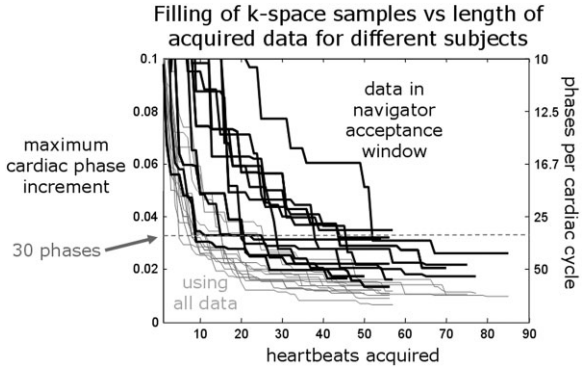

FIG. 9. Statistics of *k*-space filling maximum cardiac phase increment (described in Fig. 8) or corresponding phases per cardiac cycle vs heartbeat.

Parallel imaging is used to accelerate the initial real-time acquisition to achieve temporal resolution adequate for tracking the respiratory motion. The image domain parallel image reconstruction using the SENSE (10) algorithm results in a coil combined complex image that corresponds to a fully sampled *k*-space dataset (i.e., the missing *k*-space data are filled in). The filled-in *k*-space lines may be viewed as a convolution in *k*-space of the acquired lines, with a kernel of relatively narrow extent in *k*-space. Since the real-time acquisition used a linear phase encode order, the missing lines are filled in by a weighted sum of *k*-space samples that are acquired in close time proximity (corresponding to a few lines, spaced several ms apart). Thus, the use of parallel imaging contributes a slight temporal smear on the order of 6 ms ($\pm$pulse repetition time).

The retrospective reconstructed images have the potential to achieve an improvement in SNR compared to the raw real-time images due to effective averaging. For a given phase encode line, there is a nonuniform distribution of samples across cardiac phase. Simple cardiac rebinning was performed that consisted of averaging all samples that fell within the specified output phase, where typically 30 output phases were calculated across the cardiac cycle (i.e., 33 ms for 60 bpm). More sophisticated temporal interpolation might be useful in cases where the sampling density is lower but was not used in this work. For the parameters used in this study, the effective number of samples averaged was 7.9 ± 2.4. The number of samples averaged per bin (PE line and output phase) varies in a pseudorandom manner. The implication of this is that the noise standard deviation varies to some degree across the phase encode direction, which in theory could lead to an

altered noise appearance. However, since the variation in noise was not that significant and varied almost randomly, the noise in the retrospective reconstructed images appeared qualitatively as expected.

The proposed technique combines nonrigid motion correction with image-based navigators for selective averaging. Image-based navigators are calculated retrospectively and therefore do not permit prospective slice tracking to limit through-plane motion. Nevertheless, through-plane motion may be limited to an acceptable level based on the acceptance window. Unlike conventional navigators, the proposed approach compensates for in-plane motion and nonrigid distortion. Using conventional navigators, residual in-plane motion may lead to both loss of resolution and respiratory artifacts. In the future, there is the potential to derive image-based navigators in real time with low latency and perform prospective slice tracking, if desired.

In the work demonstrated here, a fixed acquisition period (60 sec) was used, which is considerably longer than the typical breath hold used for cine imaging. Such a long acquisition would likely limit the applicability to difficult cases for which breath-hold studies were not suitable. The actual length required to meet specific criteria such as number of samples per bin will depend on the subject's interval between R-wave peaks (RR interval) relative to sampling, as well as the respiratory gating and possible arrhythmia rejection. With real-time navigator processing, it might be possible to determine this criterion in real time and thus have the acquisition duration controlled by the imaging sequence.

The proposed approach has several benefits, including simplifying the acquisition by eliminating the time and complexity of setting up a navigator scan. Ghosting artifacts that result from residual respiratory motion during the segmented acquisition are also eliminated. Furthermore, real-time imaging is insensitive to variations in RR interval, and arrhythmia rejection may be incorporated into retrospective averaging.

In the proposed approach, images are acquired in a free running manner without ECG triggering and are retrospectively gated based on recorded ECG triggered times. It might be possible to use cardiac self-gating (22,29) and eliminate the dependence on ECG signal. While only simple arrhythmia rejection was employed for the cases studied here, retrospective processing permits the possibility of more sophisticated ECG recognition algorithms.

The retrospective reconstruction from raw data was performed in Matlab (WinXP64 version R2007a) on a PC with Intel Xeon processor at 2.66-GHz clock speed. There were approx. 540 images acquired over 60 sec. The total reconstruction time was approx. 480 sec, including parallel imaging (60 sec), image registration (11 sec), apply warp (223 sec), FFTs following motion correction (13 sec), and other navigator signal processing and rebinning calculations (173 sec). With the exception of the image registration (11 sec), all the remaining code was single threaded. The image registration portion that did not include the application of warping (image interpolation) was implemented in C-code called from Matlab and was parallelized (using eight processors). It is expected that major improvement in speed is attainable by optimizing and used of multithreading.

CONCLUSION

The proposed method provides a means of attaining high-quality cine images with many of the clinically important benefits of real-time imaging, such as free-breathing acquisition and tolerance to arrhythmias. The proposed method was validated at ~30-ms temporal resolution but could be implemented at higher effective temporal resolution (~15 ms) with longer duration acquisition. Significant SNR enhancement was achieved without apparent loss of resolution on all subjects studied. The free-breathing acquisition may be extended in duration to gain further SNR.

ACKNOWLEDGMENTS

This research was supported by the Intramural Research Program of the NIH, National Heart, Lung, and Blood Institute, and a Cooperative Research and Development Agreement between the National Heart, Lung, and Blood Institute and Siemens Medical Solutions.

REFERENCES

1. Sakuma H, Fujita N, Foo TK, et al. Evaluation of left ventricular volume and mass with breath-hold cine MR imaging. Radiology 1993;188:377–380.
2. Atkinson DJ, Edelman RR. Cineangiography of the heart in a single breath hold with a segmented turboFLASH sequence. Radiology 1991; 178:357–360.
3. Schulen V, Schick F, Loichat J, et al. Evaluation of k-space segmented cine sequences for fast functional cardiac imaging. Invest Radiol 1996; 31:512–522.
4. Epstein FH, Wolff SD, Arai AE. Segmented k-space fast cardiac imaging using an echo-train readout. Magn Reson Med 1999;41:609–613.
5. Carr JC, Simonetti O, Bundy J, et al. Cine MR angiography of the heart with segmented true fast imaging with steady-state precession. Radiology 2001;219:828–834.
6. Setser RM, Fischer SE, Lorenz CH. Quantification of left ventricular function with magnetic resonance images acquired in real time. J Magn Reson Imaging 2000;12:430–438.
7. Plein S, Smith WH, Ridgway JP, Kassner A, Beacock DJ, Bloomer TN, Sivananthan MU. Qualitative and quantitative analysis of regional left ventricular wall dynamics using real-time magnetic resonance imaging: comparison with conventional breath-hold gradient echo acquisition in volunteers and patients. J Magn Reson Imaging 2001;14:23–30.
8. Kaji S, Yang PC, Kerr AB, Tang WH, Meyer CH, Macovski A, Pauly JM, Nishimura DG, Hu BS, Rapid evaluation of left ventricular volume and mass without breath-holding using real-time interactive cardiac magnetic resonance imaging system. J Am Coll Cardiol 2001;38:527–533.
9. Hori Y, Yamada N, Higashi M, Hirai N, Nakatani S. Rapid evaluation of right and left ventricular function and mass using real-time true-FISP cine MR imaging without breath-hold: comparison with segmented true-FISP cine MR imaging with breath-hold. J Cardiovasc Magn Reson 2003;5:439–450.
10. Pruessmann KP, Weiger M, Scheidegger B, Boesiger P. SENSE: sensitivity encoding for fast MRI. Magn Reson Med 1999;42:952–962.
11. Griswold MA, Jakob PM, Heidemann RM, Nittka M, Jellus V, Wang J, Kiefer B, Haase A. Generalized autocalibrating partially parallel acqusitions (GRAPPA). Magn Reson Med 2002;47:1202–1210.
12. Kellman P, Epstein FH, McVeigh ER. Adaptive sensitivity encoding incorporating temporal filtering (TSENSE). Magn Reson Med 2001;45: 846–852.
13. Breuer FA, Kellman P, Griswold MA, Jakob PM. Dynamic autocalibrated parallel imaging using temporal GRAPPA (TGRAPPA). Magn Reson Med 2005;53:981–985.
14. Ehman RL, Felmlee JP. Adaptive technique for high definition MR imaging of moving structures. Radiology 1989;173:255–263.
15. Wang Y, Rossman PJ, Grimm RC, Riederer SI, Ehman RL. Navigator-echo-based real-time respiratory gating and triggering for reduction of respiration effects in three dimensional coronary MR angiography. Radiology 1996;198:55–60.

16. Danias PG, McConnell MV, Khasgiwala VC, Chuang ML, Edelman RR, Manning WJ. Prospective navigator correction of image position for coronary MR angiography. Radiology 1997;203:733–736.
17. Keegan J, Gatehouse P, Yang GZ, Firmin D. Coronary artery motion with the respiratory cycle during breath-holding and free-breathing: implications for slice-followed coronary artery imaging. Magn Reson Med 2002;47:476–481.
18. Larson AC, Kellman P, Arai A, Hirsch GA, McVeigh E, Li D, Simonetti OP. Preliminary investigation of respiratory self-gating for free-breathing segmented cine MRI. Magn Reson Med 2005;53:159–168.
19. Stehning C, Bornert P, Nehrke K, Eggers H, Stuber M. Free-breathing whole-heart coronary MRA with 3D radial SSFP and self-navigated image reconstruction. Magn Reson Med 2005;54:476–480.
20. Lai P, Larson AC, Park J, Carr JC, Li D. Respiratory self-gated 4D coronary MRA. In: Proceedings of the 14th Annual Meeting of ISMRM, Seattle, 2006 (Abstract 364).
21. Uribe S, Muthurangu V, Boubertakh R, Schaeffter T, Razavi R, Hill DL, Hansen MS. Whole-heart cine MRI using real-time respiratory self-gating. Magn Reson Med 2007;57:606–613.
22. Buehrer M, Curcic J, Boesiger P, Kozerke S. Prospective self-gating for simultaneous compensation of cardiac and respiratory motion. Magn Reson Med 2008;60:683–690.
23. Kellman P, Chefd'hotel C, Lorenz CH, Mancini C, Arai AE, McVeigh ER. Fully automatic, retrospective enhancement of real-time acquired cardiac cine MR images using image based navigators and respiratory motion corrected averaging. Magn Reson Med 2008;59:771–778.
24. Ledesma-Carbayo MJ, Kellman P, Arai AE, McVeigh ER. Motion corrected free-breathing delayed enhancement imaging of myocardial infarction using non-rigid registration. J Magn Reson Imaging 2007;26:184–190.
25. Chefd'hotel C, Hermosillo G, Faugeras O. A variational approach to multimodal image matching. In: Proceedings of the IEEE Workshop on Variational and Level Set Methods in Computer Vision (VLSM'2001), ICCV Workshop, Vancouver, BC, Canada, 2001.
26. Chefd'hotel C, Hermosillo G, Faugeras O. Flows of diffeomorphisms for multimodal image registration. In: Proceedings of the IEEE International Symposium on Biomedical Imaging (ISBI'2002), Washington DC, USA, 2002.
27. Feinstein JA Epstein FH, Arai AE, Foo TK, Hartley MR, Balaban RS, Wolff SD. Using cardiac phase to order reconstruction (CAPTOR): a method to improve diastolic images. J Magn Reson Imaging 1997;7:794–798.
28. Kellman P, McVeigh ER. Image reconstruction in SNR units: a general method for SNR measurement. [Published erratum in Magn Reson Med 2007;58:211–212]. Magn Reson Med 2005;54:1439–1447.
29. Larson AC, White RD, Laub G, McVeigh ER, Li D, Simonetti OP. Self-gated cardiac cine MRI. Magn Reson Med 2004;51:93-102.